

## Internal Variability in Regional Climate Downscaling at the Seasonal Scale

ADELINA ALEXANDRU

*Université du Québec à Montréal, Montréal, Québec, Canada*

RAMON DE ELIA

*Université du Québec à Montréal, and Ouranos Consortium, Montréal, Québec, Canada*

RENÉ LAPRISE

*Université du Québec à Montréal, Montréal, Québec, Canada*

(Manuscript received 12 September 2006, in final form 15 December 2006)

### ABSTRACT

To study the internal variability of the model and its consequences on seasonal statistics, large ensembles of twenty 3-month simulations of the Canadian Regional Climate Model (CRCM), differing only in their initial conditions, were generated over different domain sizes in eastern North America for a summer season. The degree of internal variability was measured as the spread between the individual members of the ensemble during the integration period. Results show that the CRCM internal variability depends strongly on synoptic events, as is seen by the pulsating behavior of the time evolution of variance during the period of integration. The existence of bimodal solutions for the circulation is also noted. The geographical distribution of variance depends on the variables; precipitation shows maximum variance in the southern United States, while 850-hPa geopotential height exhibits maximum variance in the northeast part of the domain. Results suggest that strong precipitation events in the southern United States may act as a triggering mechanism for the 850-hPa geopotential height spread along the storm track, which reaches its maximum toward the northeast of the domain. This study reveals that successive reductions of the domain size induce a general decrease in the internal variability of the model, but an important variation in its geographical distribution and amplitude was detected. The influence of the internal variability at the seasonal scale was evaluated by computing the variance between the individual member seasonal averages of the ensemble. Large values of internal variability for precipitation suggest possible repercussions of internal variability on seasonal statistics.

### 1. Introduction

It is already well established that due to the chaotic and nonlinear nature of atmospheric processes, general circulation models (GCMs) are sensitive to initial conditions (ICs; e.g., Griffies and Bryan 1997; Giorgi and Bi 2000). GCMs generate solutions of the atmospheric circulation that become significantly different after a few days of simulation when run with slightly different ICs.

Regional climate models (RCMs) are limited-area models that are driven at their lateral boundaries by reanalyses or GCM-generated data (e.g., Giorgi 1990). Their higher resolution when compared to GCMs allows for finescale details to be added upon the driving large-scale flow (e.g., Giorgi and Mearns 1991). Despite the fact that RCMs are constrained by lateral boundary conditions (LBCs), recent studies have shown that RCMs also exhibit internal variability. This variability is usually understood as the capacity of the model to produce different solutions for the same set of LBCs (von Storch 2005) and appears to vary as a function of season, domain size, and geographical location (e.g., Seth and Giorgi 1998; Giorgi and Bi 2000; Castro et al. 2005; Caya and Biner 2004; Rinke et al. 2004).

---

*Corresponding author address:* Adelina Alexandru, Département des Sciences de la Terre et de l'Atmosphère, UQAM-Ouranos, 550 rue Sherbrooke Ouest, 19<sup>e</sup> étage, Tour Ouest, Montréal, QC H3A 1B9, Canada.  
E-mail: adelina@sca.uqam.ca

As a consequence of the presence of internal variability, one may decompose any simulated climate into two components: (i) a reproducible signal associated with the external forcing (surface and LBCs) and (ii) a component due to internal variability (e.g., Ji and Vernekar 1997; Giorgi and Bi 2000; Rinke and Dethloff 2000; Wu et al. 2005). In principle, the two components could be separated, for example, by using an ensemble of the RCM simulations performed under identical conditions, except only for the conditions by which the model is initialized: deviations between such runs would reflect the degree of the internal variability of the model.

The internal variability of the model can be in some circumstances as large or larger than the external forcings. For example, differences noted in simulations of a given weather event could be interpreted as a response to changes in forcing when in reality it could be only a manifestation of the model's internal variability (e.g., Caya and Biner 2004). In the case of a change in one of the model's parameters, the information about the magnitude of the model's internal variability may allow for the assessment of the sensitivity of the response to the change of the respective parameter (e.g., Weisse et al. 2000; Christensen et al. 2001).

The investigation of RCMs' internal variability began only a few years ago, and some of the recent findings are summarized here. Weisse et al. (2000) studied the sensitivity of a limited-area model to a sea state-dependent roughness parameter by comparing two sets of experiments. They noticed that the most important differences between the two experiments occurred concurrently with episodes of high internal variability. They also found a statistically significant impact of the sea state-dependent roughness on the atmospheric circulation when the internal variability was small; the rest of the time, the impact of the sea state-dependent roughness on the atmospheric circulation appeared to be hidden by the internal variability of the model. Consequently, the authors recommended that model internal variability should be taken into account in the sensitivity test.

Giorgi and Bi (2000) analyzed an RCM's sensitivity to initial and boundary conditions over eastern Asia for a 12-month period. They added random perturbations to the ICs and LBCs of the simulations and compared the model results from the perturbed runs with those from the original simulation without perturbation. Results showed that the RCM's internal variability is insensitive to the amplitude and the type of the perturbations in the ICs. However, the RCM's internal variability seemed to be linked to the synoptic conditions,

season (maximum response in summer and minimum in winter), region, and model configuration. They also noted that, while the day-to-day model solutions were affected, the domain-wide statistics were not. The authors concluded that the internal variability is a factor that should be considered in the design, analysis, and interpretation of RCM tests.

Christensen et al. (2001) studied internal variability using two RCMs for generating an ensemble of 1-yr simulations with the same LBCs in different areas of the Mediterranean region. Their study shows that internal variability has similar magnitude in the two regional models, but geographical distributions may vary significantly. The comparison between the internal variability of RCMs with that of a GCM shows a strong dependence on the variable; for example, surface air temperature shows a much lower internal variability in an RCM than in a GCM, while evaporation and precipitation exhibit, during the European summer, comparable internal variability. The authors of this study consider that the knowledge of the internal variability enables a better assessment of the RCM simulations.

A study about the importance of the internal variability was also performed by Rinke et al. (2004) for a 1-yr simulation with a pan-Arctic RCM. The magnitude of the internal variability was measured by the monthly and seasonal-mean pattern differences and the root-mean-square differences (RMSDs). For this particular region, results show an internal variability that is generally larger than that reported earlier with midlatitude domains. Their results show that the model response to a perturbation does not depend strongly on the type and magnitude of the perturbation, which is in agreement with results obtained by Giorgi and Bi (2000) for midlatitude domains. Unlike Giorgi and Bi (2000), however, their (Rinke et al.) results show that the maximum response was found in autumn-winter with smaller variability in summer. They explained this behavior of the internal variability by the Arctic atmospheric circulation and planetary waves activity being weaker during the summer. During the winter and autumn, large-scale Arctic circulation is dominated by a strong zonally symmetric flow that hinders the migration of the weather systems out of the circumpolar domain. The authors conclude that the pronounced magnitude of the internal variability must be taken into account when discussing the climate signal in Arctic RCMs.

Caya and Biner (2004) performed a three-member ensemble of 1-yr simulations initialized differently over a large midlatitude domain with the aim of studying Canadian Regional Climate Model (CRCM) internal

variability. Results show two distinct seasonal behaviors: in winter all simulations exhibited very weak internal variability, while in summer large differences are noted between pairs of simulations. Over midlatitudes in summer, the slower upper-tropospheric winds appear to reduce the control exerted by the LBCs on the simulations within the domain. In addition, the stronger local processes (such as convection) could explain the higher values of the internal variability in summer. The authors also remarked that, although the evolution of the various weather systems can be quite different, the seasonal means of each simulation were similar.

Vannitsem and Chomé (2005) investigated the impact of domain size on RCM simulations. Seven domain sizes centered over western Europe were chosen for a 40-day sensitivity test with the Eta RCM. Results show that small perturbations in the ICs and the surface fields do not significantly change the model solution for small domains, suggesting that the variability around the attractor of the solution for a given set of LBCs is very small. The experiment for larger domains, however, revealed significant differences among the trajectories of the simulations, suggesting a large variability of model solutions.

Lucas Picher et al. (2004) also tested the influence of domain size on internal variability. Based on results of two 5-yr simulations initialized differently for two different domain sizes covering eastern North America and part of the Atlantic Ocean, they found that internal variability has low values for the small domain. Contrary to previous results, however (Giorgi and Bi 2000; Christensen et al. 2001; Caya and Biner 2004), they found that large internal variability occurred during the winter season for the large domain.

The present work continues the research on internal variability, giving special emphasis to the geographical variations of the internal variability during the model's integration on different domain sizes. The first step consists of evaluating of the number of ensemble members required to obtain a robust estimation of the internal variability. Later, we use this finding to describe the main features of the time evolution and geographical distribution of internal variability at an instantaneous and seasonal scale and its sensitivity to domain size. Finally, we focus on particular cases where there seem to exist two attractors of the RCM solution for a set of LBCs.

The work is organized as follows. Section 2 briefly describes the CRCM, the simulation setup, and the evaluation methods. Results are presented in section 3, and the concluding remarks are discussed in section 4.

## 2. The CRCM and experimental design

### a. Model description

The model used in the present study is version 3.6.1 of the Canadian RCM (CRCM; Caya and Laprise 1999). The CRCM is a limited-area model based on the fully compressible Euler equations solved by a semi-implicit and semi-Lagrangian numerical scheme (Bergeron et al. 1994; Laprise et al. 1997). The model uses the physical parameterization package of the second-generation CGCM (GCMii; McFarlane et al. 1992) except for the Bechtold–Kain–Fritsch deep and shallow convective parameterizations (Kain and Fritsch 1990; Bechtold et al. 2001). The computational points are fixed on a three-dimensional staggered grid projected onto polar-stereographic coordinates in the horizontal and Gal-Chen terrain-following levels in the vertical (Gal-Chen and Sommerville 1975).

To define the initial state, the CRCM requires information for the following atmospheric fields: horizontal winds, vertical motion, temperature, surface pressure, and specific humidity. These atmospheric fields are also required at each time step at the lateral boundaries of the model domain. Nudging is applied on the horizontal wind components over a relaxation zone of 10 grid points near the lateral boundary where the CRCM-simulated winds are relaxed toward the values of the driving data (Davies 1976). In the present study, the necessary atmospheric ICs and LBCs are provided by National Centers for Environmental Prediction–National Center for Atmospheric Research (NCEP–NCAR) data available every 6 h. Fields provided at the boundaries are linearly interpolated in time for each time step (Kalnay et al. 1996). In addition, the CRCM requires ICs for the following land surface variables: surface temperature, liquid and frozen soil water fraction, and snow amount and snow age. Ocean surface variables are prescribed from Atmospheric Model Intercomparison Project (AMIP) data (Fiorino 2004).

### b. Simulation setup

Figure 1 presents the domains and topography used for the CRCM simulations in the present study. Five model domains cover eastern North America and part of the Atlantic Ocean at approximately 45-km resolution with sizes varying from  $140 \times 140$  to  $80 \times 80$  grid points. In the vertical, 18 Gal-Chen levels are distributed from the ground to the model's lid at 30 km. The CRCM uses a 15-min time step. It is important to mention that, although the model has the option of spectral nudging (e.g., von Storch et al. 2000; Riette and Caya 2002), this capability was not used in order to appreciate the internal variability in its basic state.

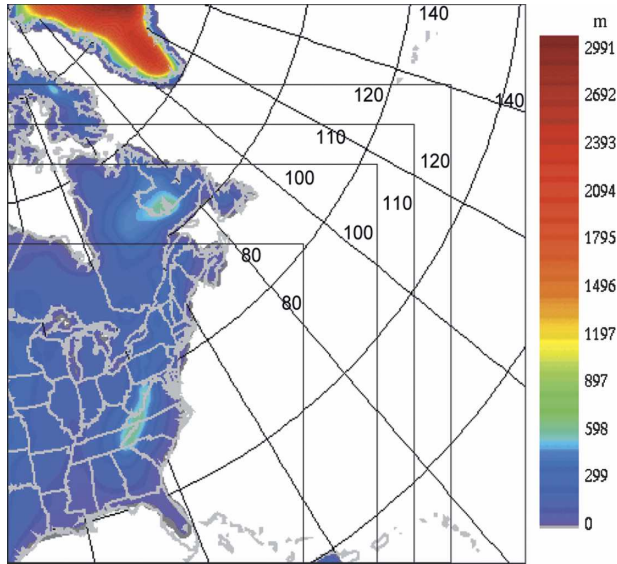


FIG. 1. CRCM computational domains and topography (m).

Ensembles of 20-member simulations were performed over five different domain sizes. All integrations started with ICs 1 day apart between 0000 UTC 1 May 1993 and 0000 UTC 20 May 1993; all simulations ended on 0000 UTC 1 September 1993, so that the 20 simulations overlap for the 3 months of June–August 1993, with a spinup period varying from 11 to 30 days. The integrations share exactly the same LBCs for the atmospheric fields and the same prescribed SST and sea ice coverage for the ocean surface; the only difference is in a delay of 24 h at the beginning of each run of the ensemble.

### c. Evaluation methods

Internal variability of the model will be measured by the spread among the ensemble members during the integration period, using the standard deviation ( $\sqrt{\sigma_{\text{en}}^2}$ ) between the 20 members in the ensemble of simulations, where  $\sigma_{\text{en}}^2$  is the variance estimated as

$$\sigma_{\text{en}}^2(i, j, k, t) = \frac{1}{M} \sum_{m=1}^M [X_m(i, j, k, t) - \langle X \rangle(i, j, k, t)]^2. \quad (1)$$

The term  $X_m(i, j, k, t)$  refers to the value of a variable  $X$  on grid point  $(i, j, k)$  at time  $t$  for member  $m$  in the ensemble and  $M$  is the total number of ensemble members. The term  $\langle X \rangle(i, j, k, t)$  is the ensemble mean defined as

$$\langle X \rangle(i, j, k, t) = \frac{1}{M} \sum_{m=1}^M X_m(i, j, k, t). \quad (2)$$

A measure of the domain-averaged internal variability during the course of the model integration is provided by the square root of the spatially averaged variance ( $\sqrt{\sigma_{\text{en}}^{2-xy}}$ ), where  $\sigma_{\text{en}}^{2-xy}$  is computed as

$$\sigma_{\text{en}}^{2-xy}(k, t) = \frac{1}{I \times J} \sum_{j=1}^J \sum_{i=1}^I \sigma_{\text{en}}^2(i, j, k, t), \quad (3)$$

with  $I$  and  $J$  the numbers of grid points along  $x$  and  $y$ , respectively, over the domain of interest. The 3-month time average of the internal variability and its spatial distribution in the domain for the entire season are provided by the square root of the time-averaged variance ( $\sqrt{\sigma_{\text{en}}^{2-t}}$ ), where  $\sigma_{\text{en}}^{2-t}$  is defined as

$$\sigma_{\text{en}}^{2-t}(i, j, k) = \frac{1}{N} \sum_{t=1}^N \sigma_{\text{en}}^2(i, j, k, t), \quad (4)$$

where  $N$  refers to the number of archived time steps in the period of interest ( $N = 369$  time steps for the three summer months at 6-h intervals). We also use in our estimations spatially averaged time-averaged internal variability defined as the square root of the domain-averaged time-averaged variance  $\sqrt{\sigma_{\text{en}}^{2-t-xy}}$ , where  $\sigma_{\text{en}}^{2-t-xy}$  is provided by

$$\sigma_{\text{en}}^{2-t-xy}(k) = \frac{1}{I \times J \times N} \sum_{j=1}^J \sum_{i=1}^I \sum_{t=1}^N \sigma_{\text{en}}^2(i, j, k, t). \quad (5)$$

The influence of internal variability at the seasonal scale is appreciated by the variation of the seasonal-mean field. The spread between the seasonal averages of the ensemble members is estimated as the square root of the variance between the individual member seasonal averages ( $\sqrt{\sigma_s^2}$ ), where  $\sigma_s^2$  is computed as

$$\sigma_s^2(i, j, k) = \frac{1}{M} \sum_{m=1}^M [\bar{X}_m^t(i, j, k) - \langle \bar{X} \rangle^t(i, j, k)]^2, \quad (6)$$

where  $\bar{X}_m^t(i, j, k)$  is the seasonal average of member  $m$  and  $\langle \bar{X} \rangle^t(i, j, k)$  is the seasonal average of the ensemble mean. The relative importance of the internal variability on the seasonal mean is provided by the coefficient of the variation ( $I$ ) computed as

$$I(i, j, k) = \frac{\sqrt{\sigma_s^2(i, j, k)}}{\langle \bar{X} \rangle^t(i, j, k)}. \quad (7)$$

This measure will be particularly useful for the precipitation field.

A measure for the domain-averaged departure of the individual simulations from the ensemble mean is obtained by computing root-mean-square differences (RMSDs) as

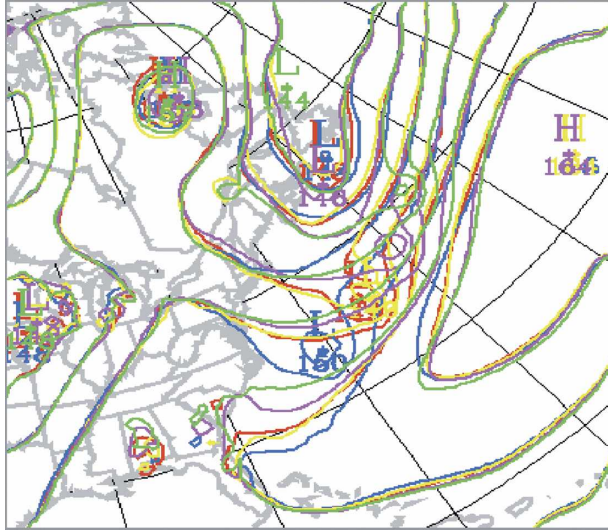


FIG. 2. Five members of the CRCM runs with a delay of 24 h in their ICs (0000 UTC 1 May–0000 UTC 5 May 1993) for the 850-hPa geopotential height (dam) valid at 0000 UTC 25 Jul 1993.

$$\text{RMSD}_m(k, t) = \sqrt{[X_m(i, j, k, t) - \langle X \rangle(i, j, k, t)]^2}^{xy} \quad (8)$$

These statistics will be evaluated excluding the spinup period and removing the 10-point relaxation zone. The study will focus on precipitation and 850-hPa geopotential height.

### 3. Results and analysis

We will begin by evaluating the number of members required for a stable estimate of the internal variability (section 3a). The spatial pattern and the temporal variation of internal variability will be investigated in section 3b and their sensitivity to domain size will be discussed in section 3c. At the end of this section we will present two particular cases of bimodal solutions (section 3d).

#### a. Ensemble size experiment

Figure 2 shows for 850-hPa geopotential height an example of five ensemble members valid at 0000 UTC 25 July 1993. It can be noticed that, in certain areas, especially toward the center of the domain, the model produces different solutions for the same set of boundary conditions.

Due to computational cost, several earlier studies of internal variability were based on small ensembles, generally with two to four members (e.g., Giorgi and Bi 2000; Caya and Biner 2004). One of the first aims of our study was to investigate the impact of a small ensemble

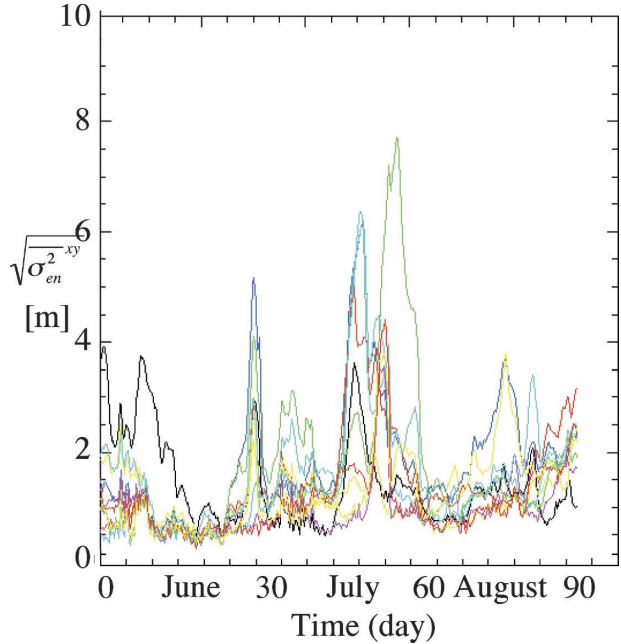


FIG. 3. Ensemble-size experiment: time evolution of domain-averaged variability ( $\sqrt{\sigma_{en}^2}^{xy}$ ) for 10 different two-member ensembles for the 850-hPa geopotential height (m).

on the estimation of the CRCM internal variability. Hence, the model's internal variability is first estimated using 10 different sets of two members taken randomly from the 20-member ensemble for a  $120 \times 120$  grid-point domain (which is a conventional domain size). Figure 3 shows the time evolutions of the domain-averaged 850-hPa geopotential height variability ( $\sqrt{\sigma_{en}^2}^{xy}$ ) [as defined in (3)] for 10 different two-member ensembles. Significant differences can be noted between these 10 time series, in both the amplitude and the timing of the domain-averaged variability. Particularly telling is the variety of maxima on geopotential height toward the end of July. The differences in the geographical distribution of the internal variability from these two-member estimations persist even after their averaging for the entire season, as shown in the example of Fig. 4 for  $\sqrt{\sigma_{en}^2}^t$  [as defined in (4)]. While the maximum is located toward the northeast of the domain in all cases, significant differences in magnitude and geographical distribution are clearly visible among the estimates.

To establish the minimum ensemble size required for a robust estimation of internal variability, a series of experiments was carried out by progressively increasing the ensemble size. Figure 5 shows the domain-averaged, time-averaged 850-hPa geopotential height variability ( $\sqrt{\sigma_{en}^2}^t$ ) [as defined in (5)] obtained from

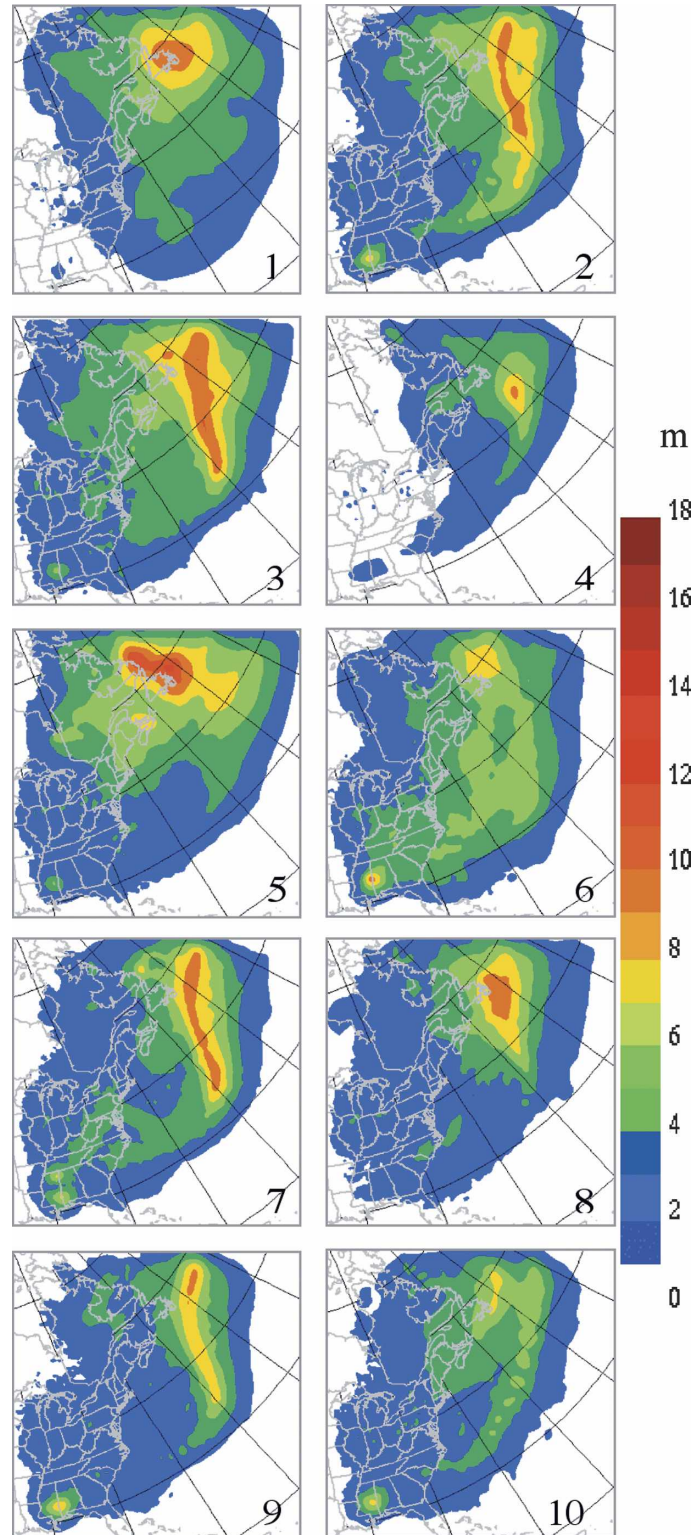


FIG. 4. Ensemble-size experiment: time-averaged variability ( $\sqrt{\sigma_{\text{cn}}^2}$ ) of the 850-hPa geopotential height (m) for 10 different two-member ensembles.

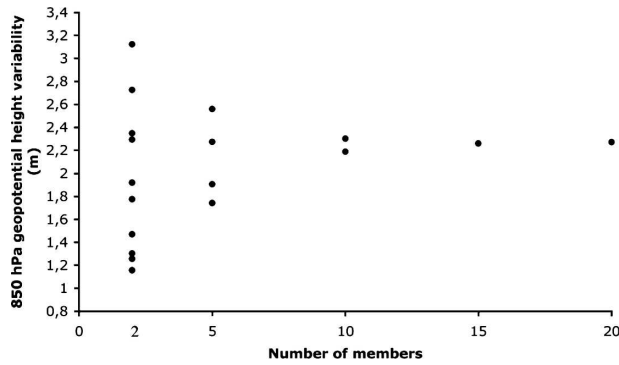


FIG. 5. Ensemble-size experiment: variation of the 850-hPa geopotential height domain-averaged, time-averaged internal variability ( $\sqrt{\sigma_{en}^{2-xy}}$ ) with the ensemble size for 10 independent ensembles of 2 simulations, 4 independent ensembles of 5 simulations, 2 independent ensembles of 10 simulations, 1 ensemble of 15 simulations, and 1 ensemble of 20 simulations.

ensembles of various sizes. The figure shows that small ensembles of two or five members lead to a large spread of internal variability values whereas larger ensembles (10, 15, or 20 members) readily converge toward a stable value. Good agreement in time-averaged internal variability ( $\sqrt{\sigma_{en}^{2-t}}$ ) (Fig. 6) and in the variability of the seasonal mean ( $\sqrt{\sigma_s^2}$ ) (not shown) is noted for the large ensembles (10, 15, and 20 members). Twenty members appear to provide a fairly robust estimate of the internal variability. A larger ensemble size would have undoubtedly improved the estimation of the internal variability, especially on an instantaneous basis, but this would have limited our computing ability to perform tests with different domain sizes, as reported in section 3c.

*b. Geographical distribution and time evolution of the internal variability*

It is informative to study the evolution of the internal variability for a specific time period. Figure 7 shows the

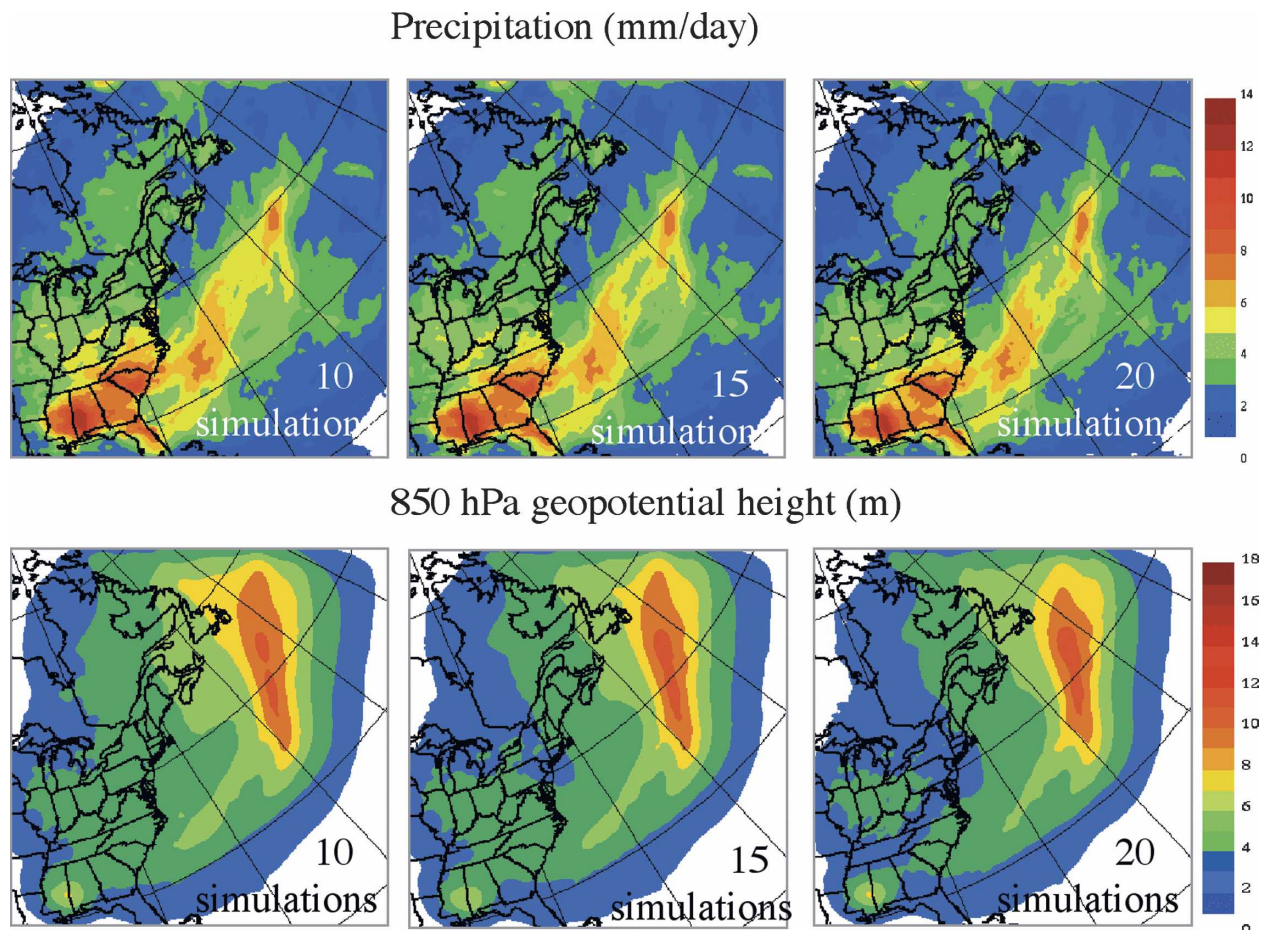


FIG. 6. Ensemble-size experiment: time-averaged variability ( $\sqrt{\sigma_{en}^{2-t}}$ ) of three ensembles composed of 10, 15, and 20 members for (top) the precipitation ( $\text{mm day}^{-1}$ ) and (bottom) 850-hPa geopotential height (m).

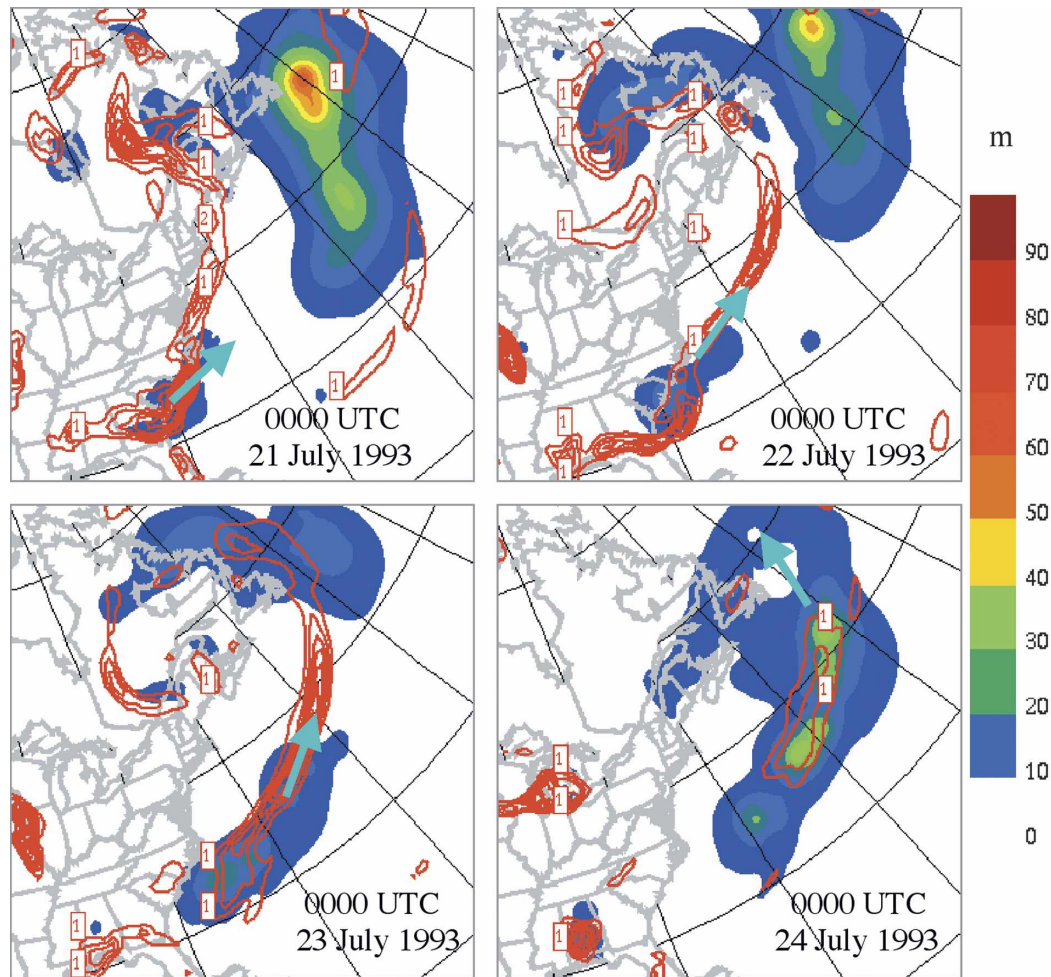


FIG. 7. Internal variability experiment (domain  $120 \times 120$ ): 4-day time evolution of ensemble-mean precipitation ( $\text{mm day}^{-1}$ ; red contour) and 850-hPa geopotential height variability ( $\sqrt{\sigma_{\text{en}}^2}$ ) (dam; color). The colored arrow indicates the trajectory of the  $\sqrt{\sigma_{\text{en}}^2}$  displacement along the storm track.

ensemble-mean precipitation and the variability of the 850-hPa geopotential height  $\sqrt{\sigma_{\text{en}}^2}$  [as defined in (1)] during 4 days in July 1993 (from 0000 UTC 21 July to 0000 UTC 24 July). On 21 July 1993, large 850-hPa geopotential height  $\sqrt{\sigma_{\text{en}}^2}$  values (50 m) are noticed in the northeast part of the domain. An evaluation of the time evolution of the 850-hPa geopotential height and precipitation shows that the spread among the simulations had actually been developing along the storm track 4 days before (18 July 1993) concurrently with heavy precipitation simulated in the southern United States (not shown). On 21 July 1993, a new maximum of variability could also be seen over Georgia and South Carolina, and collocated with it there was a region of heavy precipitation that had begun a day earlier. In the following days that maximum variability center intensified and moved northeastward (as indi-

cated by the blue arrow in Fig. 7). On 24 July 1993, a new center of geopotential variability developed over Alabama, associated with another heavy precipitation event there. These cases suggest that large geopotential height internal variability could be found downstream of regions of heavy precipitation. Although this pattern was repeated a few times and tended to dominate the seasonal average, other mechanisms were present too.

The magnitude and geographical distribution of the internal variability appear to vary greatly during the 3 months of this study. As an illustration, Fig. 8 shows weekly mean values for four specific weeks during the summer season. During the first week of June, very little internal variability in the precipitation is registered, while geopotential height is more active toward the northeast. The last week of June partially resembles

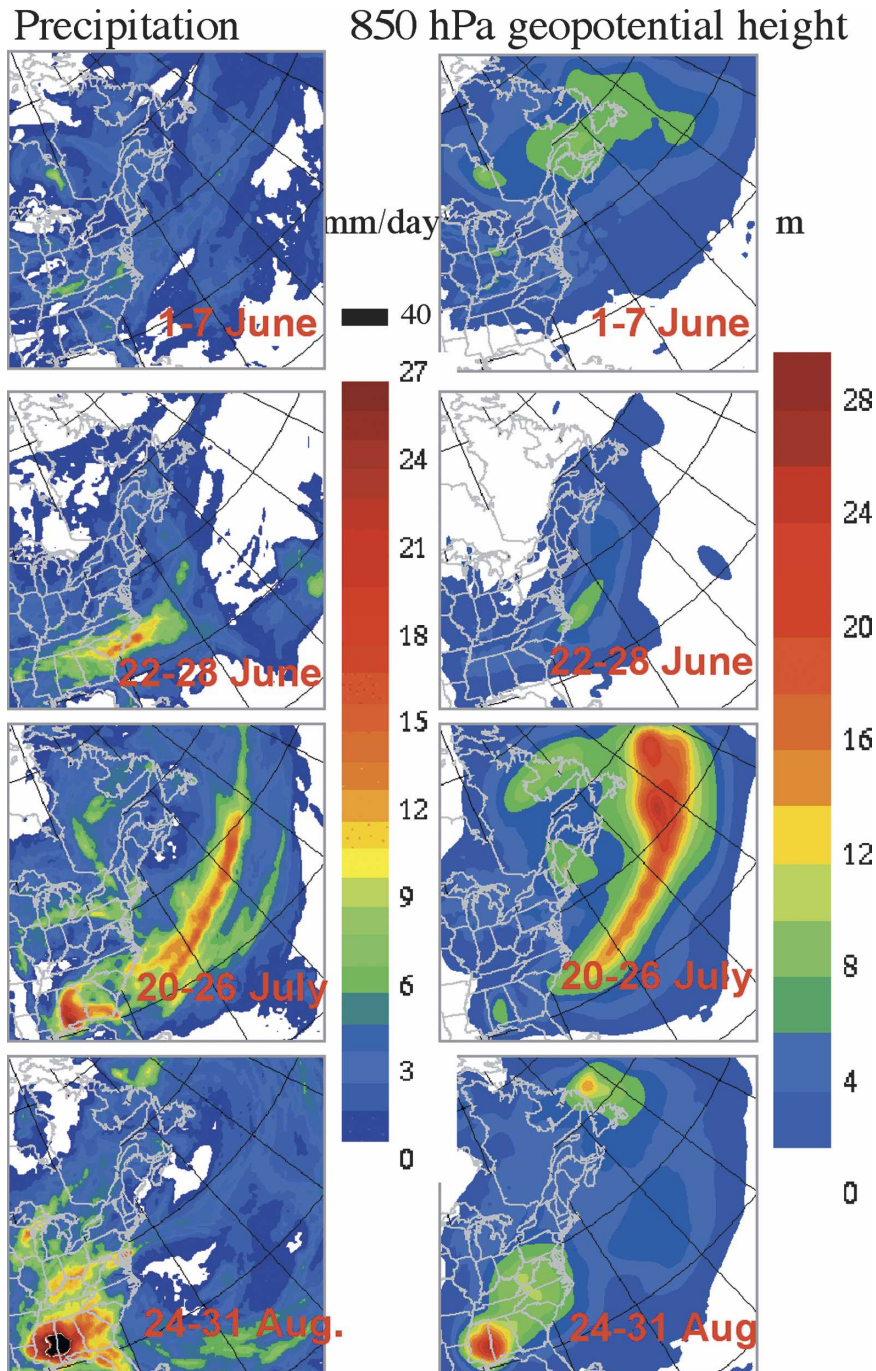


FIG. 8. Internal variability experiment (domain  $120 \times 120$ ): weekly averaged variability ( $\sqrt{\sigma_{cn}^2}$ ) corresponding to four weeks of summer season for the precipitation ( $\text{mm day}^{-1}$ ; left-side panels) and for the 850-hPa geopotential height (m; right-side panels).

the strong activity of late July, although the area of internal variability did not seem to propagate downstream as in July. The strong signal over the Mississippi River valley during the August week was caused by a slow-moving hurricane-like system that achieved

various levels of intensity in the different members [the large variabilities during the weeks of 13–19 July (not shown) and 20–26 July (Fig. 8) contribute heavily to the 3-month mean variability shown earlier in Fig. 6].

## Precipitation      850-hPa Geopotential height

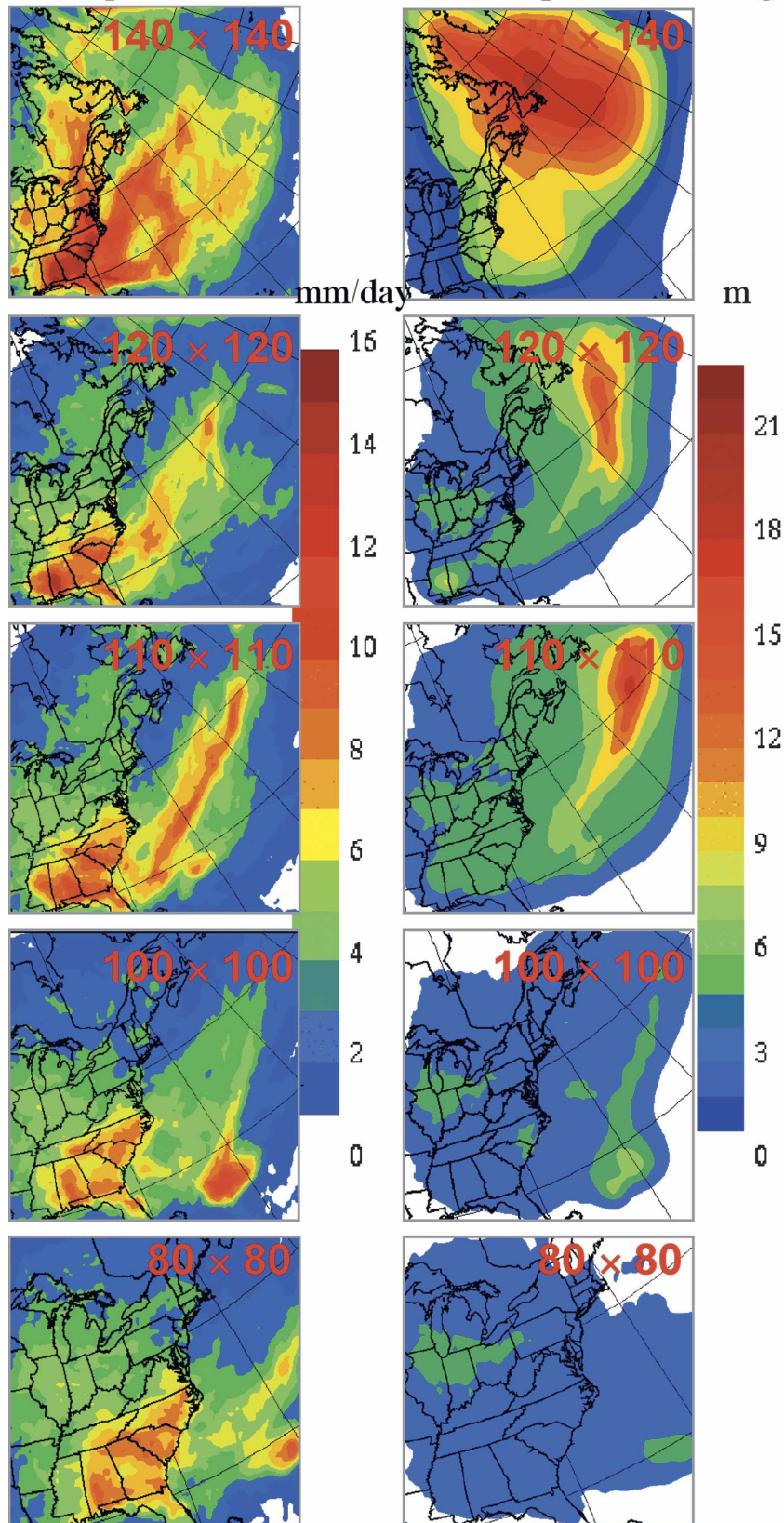


FIG. 9. Internal variability experiment (20-member ensembles on a set of different model domain sizes): time-averaged variability ( $\sqrt{\sigma_{\text{en}}^2}$ ) computed for (left) each domain size for the precipitation ( $\text{mm day}^{-1}$ ) and (right) for the 850-hPa geopotential height (m).

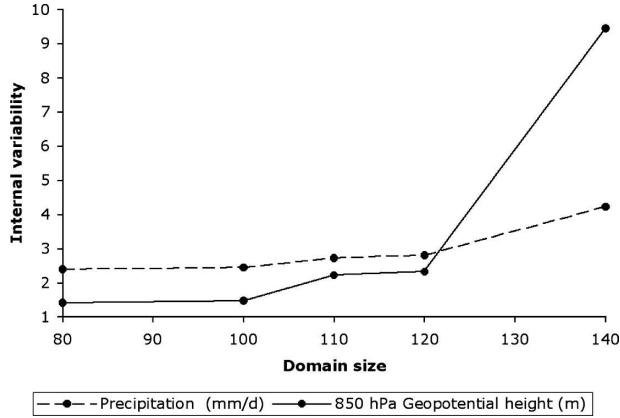


FIG. 10. Internal variability experiment (20-member ensembles on a set of different model domain sizes): variation of the domain-averaged time-averaged internal variability ( $\sqrt{\sigma_{\text{en}}^2}$ ) with the domain size for the precipitation (mm day<sup>-1</sup>; dash curve) and 850-hPa geopotential height (m; continuous curve).

### c. Influence of the domain size on the RCM internal variability

Experiments have been performed with five different domain sizes to study the influence of the domain size on the internal variability. Given the apparent role of the convection in the southern United States in triggering the internal variability, all domains are defined as keeping the southwest corner fixed (Fig. 1).

Figure 9 shows the time-averaged internal variability ( $\sqrt{\sigma_{\text{en}}^2}$ ) [as defined in (4)] for the precipitation and the 850-hPa geopotential height, for various domain sizes. In general, larger domains lead to larger internal variability, although the increase in magnitude is not monotonic at each geographical location. For example, the 100 × 100 domain exhibits more intense internal variability of precipitation and geopotential height over the ocean east of Florida than do the larger 110 × 110 or 120 × 120 domains. A detailed synoptic analysis of the simulations reveals that the 100 × 100 domain size developed in that region a tropical storm that lasted for about 4 days and showed a high level of internal variability. This system did not develop for the other domain sizes. Excluding these 4 days, the simulations on the different domain sizes were rather similar. Yet, the influence of these 4 days is non-negligible in the 3-month time average of the internal variability ( $\sqrt{\sigma_{\text{en}}^2}$ ).

Figure 10 shows the variation of the domain-averaged time-averaged internal variability ( $\sqrt{\sigma_{\text{en}}^2}$ ) [as defined in (5)] with domain size. The aforementioned general increase in the internal variability with domain size is noted, although the increase is not quite

monotonic and is rather different for different variables. This absence of monotonic growth of the internal variability with domain size might simply be the result of sampling noise. A study with a larger number of summer seasons is needed to verify this hypothesis.

The influence of the domain size on the variability of the seasonal mean ( $\sqrt{\sigma_s^2}$ ) [as defined in (6)] is shown in Fig. 11. As for  $\sqrt{\sigma_{\text{en}}^2}$ , the  $\sqrt{\sigma_s^2}$  tends to increase with domain size, but not uniformly.

It is important to note that varying the domain size not only modifies the internal variability, but it also modifies the time average of most fields (e.g., Seth and Giorgi 1998). A quantitative estimation of the uncertainty associated with the arbitrary choice of domain size can be obtained from the square root of the domain-size variance ( $\sqrt{\sigma_D^2}$ ), where  $\sigma_D^2$  is estimated as

$$\sigma_D^2(i, j, k) = \frac{1}{N} \sum_{n=1}^N \{ \overline{\langle X \rangle}_n^t(i, j, k) - [\overline{\langle X \rangle}^t(i, j, k)] \}^2, \quad (9)$$

where the term  $\overline{\langle X \rangle}_n^t(i, j, k)$  refers to the ensemble-mean seasonal average of a simulated field on domain  $n$ ; the term without the subscript  $[\overline{\langle X \rangle}^t(i, j, k)]$  refers to the average of the  $N$  domains; hence,

$$[\overline{\langle X \rangle}^t(i, j, k)] = \frac{1}{N} \sum_{n=1}^N \overline{\langle X \rangle}_n^t(i, j, k), \quad (10)$$

where  $N$  is the number of domains (in our case, five different domains with sizes between 140 × 140 and 80 × 80 grid points; cf. Fig. 1). We also estimated, for the precipitation field, the interdomain coefficient of variation ( $I_D$ ) as

$$I_D(i, j, k) = \frac{\sqrt{\sigma_D^2(i, j, k)}}{[\overline{\langle X \rangle}^t(i, j, k)]}. \quad (11)$$

For this study, even though the integrations are performed using different domain sizes, the statistics are evaluated only over a diagnostic area corresponding to that of the smallest domain.

Figure 12 shows the precipitation ensemble means over the diagnostic area of all five domains. Changes in the precipitation mean are noticeable for certain areas over the southern United States with each reduction in the domain size, especially in the Tennessee area, where the  $\sqrt{\sigma_D^2}$  [as defined in (9)] reaches 2 mm day<sup>-1</sup> with a corresponding interdomain coefficient of variation  $I_D$  [as defined in (11)] of about 36% (Fig. 13). In the case of the 850-hPa geopotential height (Fig. 14), the  $\sqrt{\sigma_D^2}$  maximum (about 10 m) is however found toward the northeast corner of the diagnostic area.

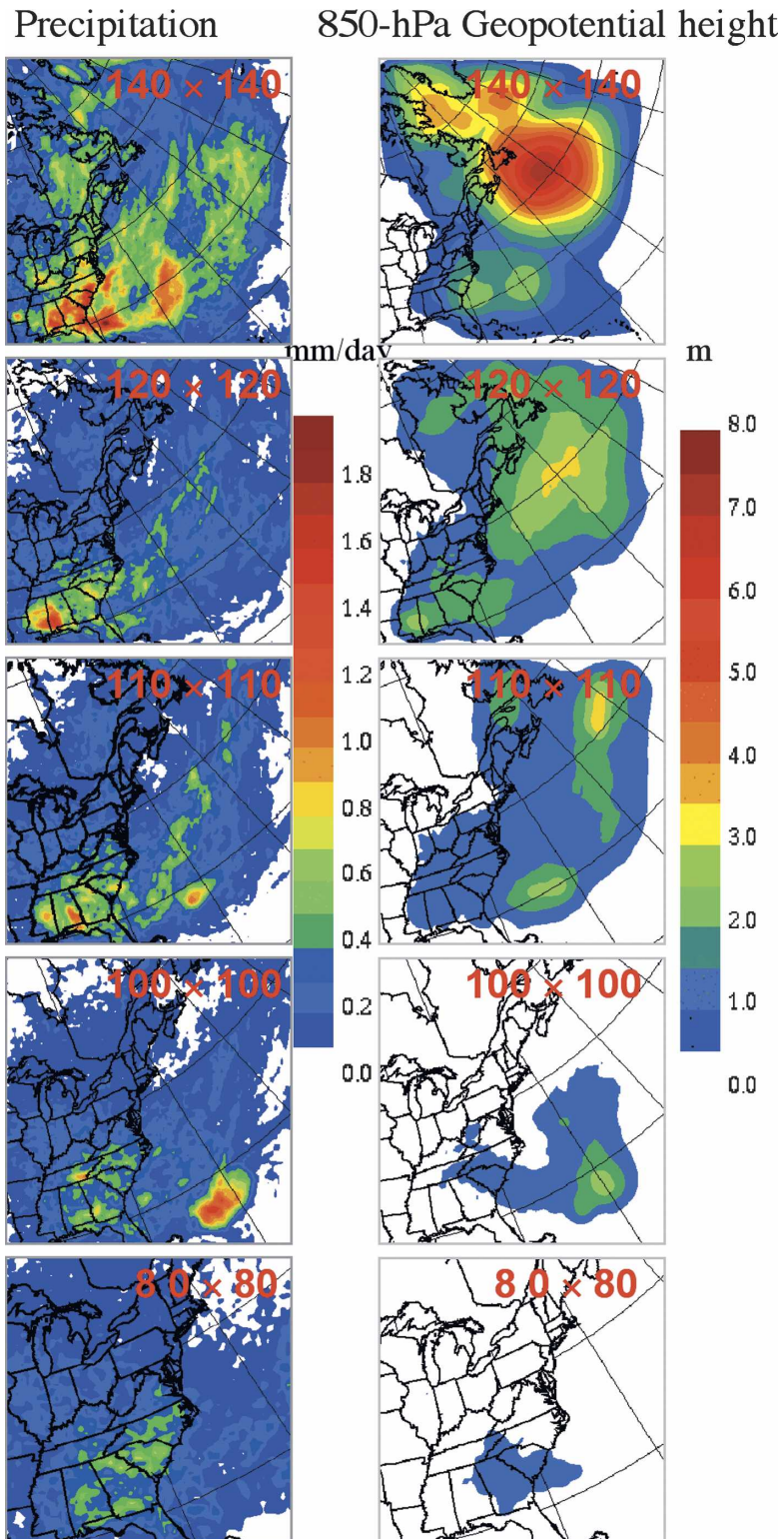


FIG. 11. Internal variability experiment (20-member ensembles on a set of different domain sizes): variability of the seasonal-mean ( $\sqrt{\sigma_x^2}$ ) computed for (left) each domain size for the precipitation ( $\text{mm day}^{-1}$ ) and (right) for the 850-hPa geopotential height (m).

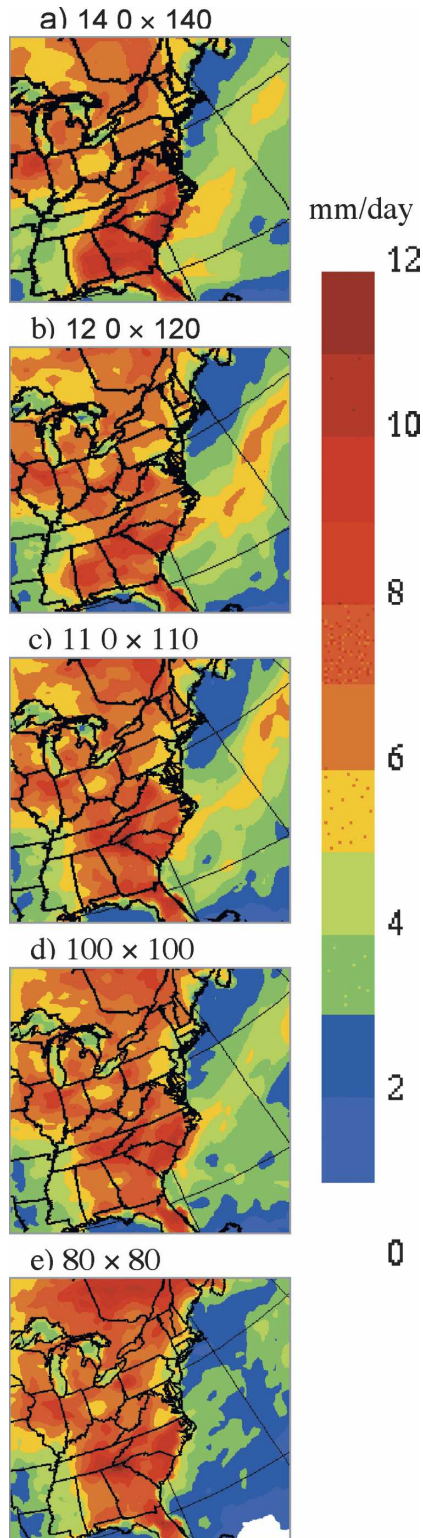


FIG. 12. Variability with domain size of the seasonal ensemble mean computed from ensembles of 20 simulations on different model domain sizes: precipitation ensemble mean ( $\text{mm day}^{-1}$ ) on domain sizes of (a)  $140 \times 140$ , (b)  $120 \times 120$ , (c)  $110 \times 110$ , (d)  $100 \times 100$ , and (e)  $80 \times 80$  grid points.

It can be seen by comparing Figs. 13 and 11 that the uncertainty introduced in the time average due to choice options in domain size are, in general, comparable to the internal variability of the larger domain, and bigger than that of the other domains. Over Tennessee, however, this is not the case: interdomain variability is much larger than that of the internal variability of any domain.

Sensitivity to domain size in the time average has received some attention (e.g., Castro et al. 2005), and it has been shown that large-scale nudging (e.g., Weisse and Feser 2003) can considerably reduce these effects.

#### d. Clustering of solutions on different attractors

Close synoptic inspection of the time evolution of each member in the ensemble has revealed a tendency for subsets of the members' solutions to cluster around some distinct states, which we will refer to as attractors. Figure 15 shows the case of bimodal behavior of the solutions in the time evolution of the 850 hPa-geopotential height on the  $120 \times 120$  domain. The separation of the members into two groups has been made subjectively. During 19–22 July, the model's internal variability ( $\sqrt{\sigma_{\text{en}}^2}$ ) [as defined in (1)] was quite large (48 m). The 20 members appeared to separate quite naturally into a group of 5 members and another group of 15 members as seen in Fig. 15. The low pressure system off of the East Coast appears to have two distinct preferred locations, a distance of some 600 km from one another. The clustering of the solutions has an effect on the  $\sqrt{\sigma_{\text{en}}^2}$  values (shown in the right-hand panels of Fig. 15), which show distinct maxima (48 m) around the "attractor." At a later time (0000 UTC 25 July 1993), one member stands out from the rest of the ensemble (Fig. 16; see Fig. 17 for the  $120 \times 120$  domain). Such separation around different attractors did not occur for domains that were  $100 \times 100$  grid points and smaller (not shown). Another bimodal solution appears on the  $140 \times 140$  domain (Fig. 17), but it will not be discussed in detail.

The existence of bimodal solutions could be the consequence of dynamical conditions that favor certain states, as shown for example by Plu and Arbogast (2005). It does not seem plausible that bimodality is the result of the manner in which the perturbations to the initial conditions are produced. The reason for this belief is that the perturbations were constructed by simply varying the starting time and hence without favoring the growth of any particular mode. In addition, bimodal solutions appear long after—around 2 months—the starting time. The possibility that bimodality may be the result of poor sampling of the distribution (only 20 members) should not be discounted.

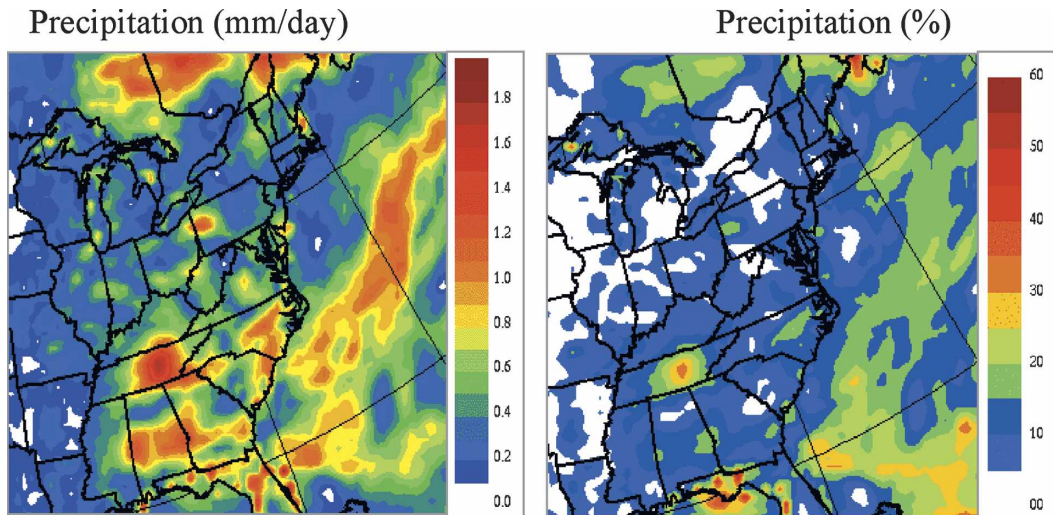


FIG. 13. Variability with domain size of the ensemble-mean seasonal mean, computed from ensembles of 20 simulations on different model domain sizes: (left) precipitation interdomain variability ( $\sqrt{\sigma_D^2}$ ) ( $\text{mm day}^{-1}$ ) and (right) precipitation coefficient of variation ( $I_D$ ) (%). Statistics were computed over the diagnostic area.

## 850-hPa Geopotential height (m)

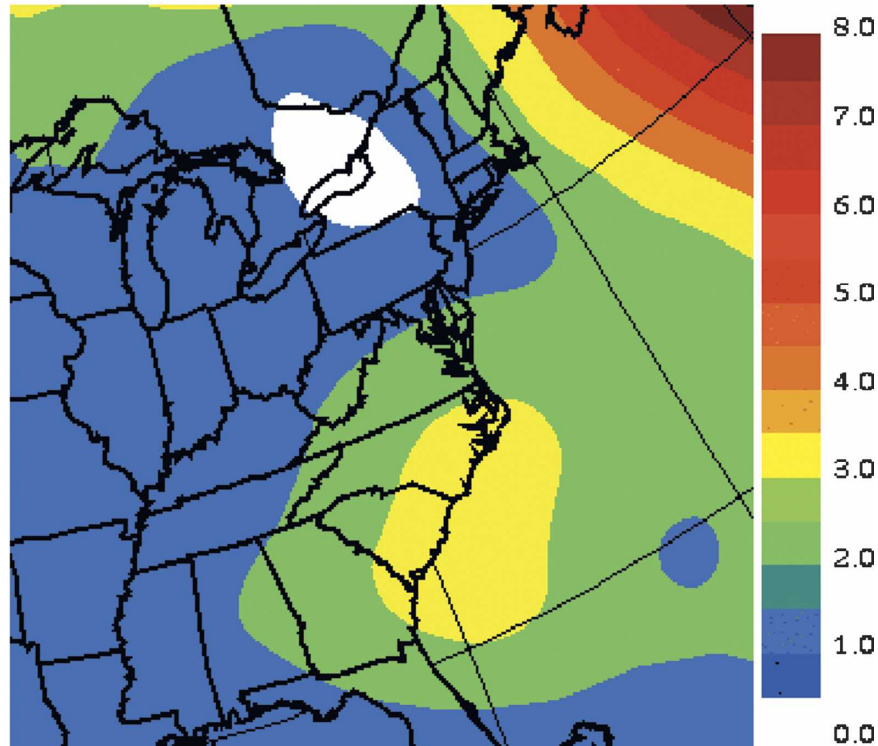


FIG. 14. Variability with domain size of the ensemble-mean seasonal mean, computed from ensembles of 20 simulations on different model domain sizes: 850-hPa geopotential height  $\sqrt{\sigma_D^2}$  (m). Statistics were computed over the diagnostic area.

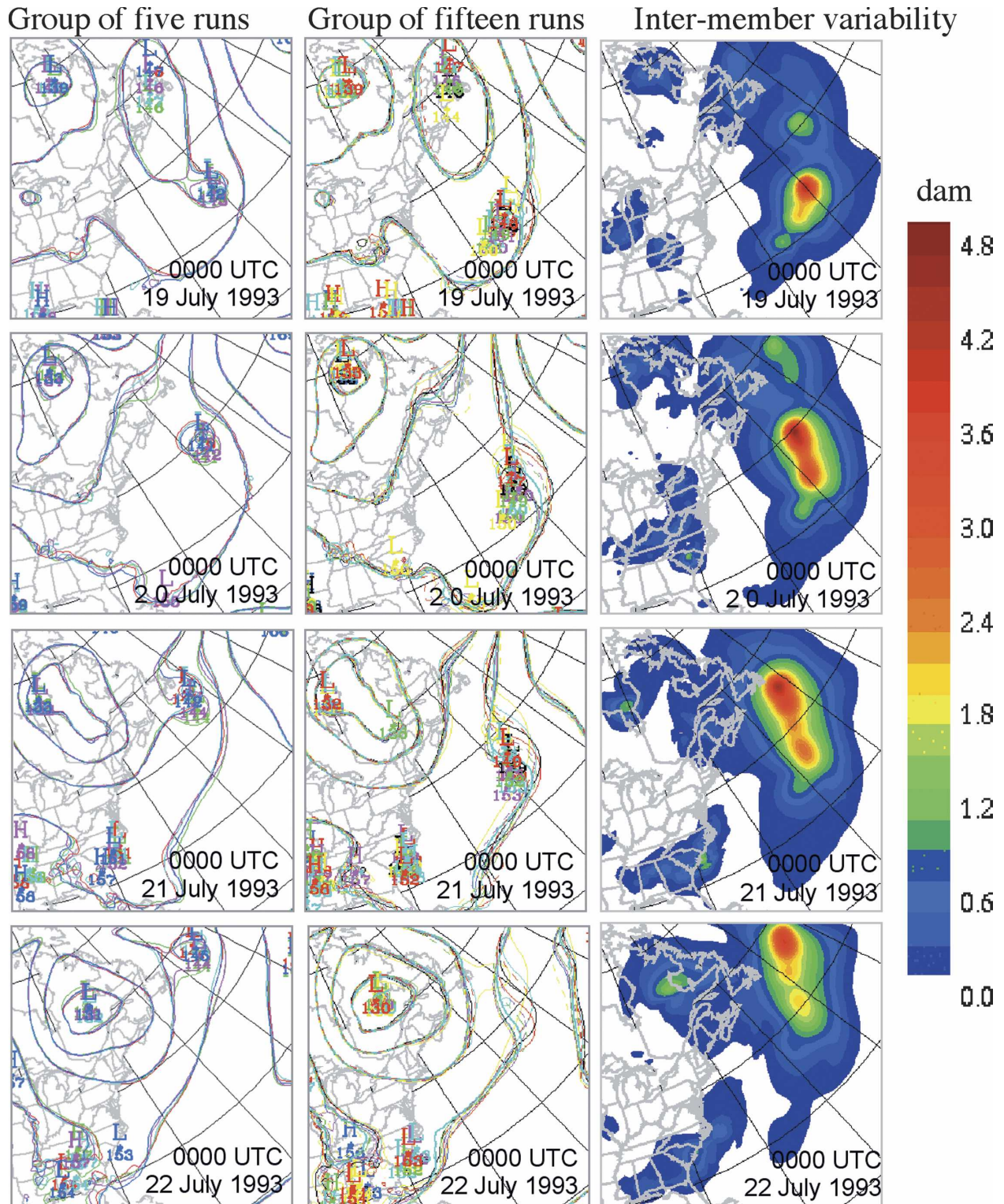


FIG. 15. Bimodal solutions (20-member ensemble, domain  $120 \times 120$ ): the 20 members of the ensemble appeared to separate into a group of (left) 5 simulations and (middle) 15 simulations during the integration of the 850-hPa geopotential height (dam); (right) the intermember variability  $\sqrt{\sigma_{\text{en}}^2}$  (dam) for this particular case (valid at 0000 UTC 19 Jul–0000 UTC 22 Jul 1993).

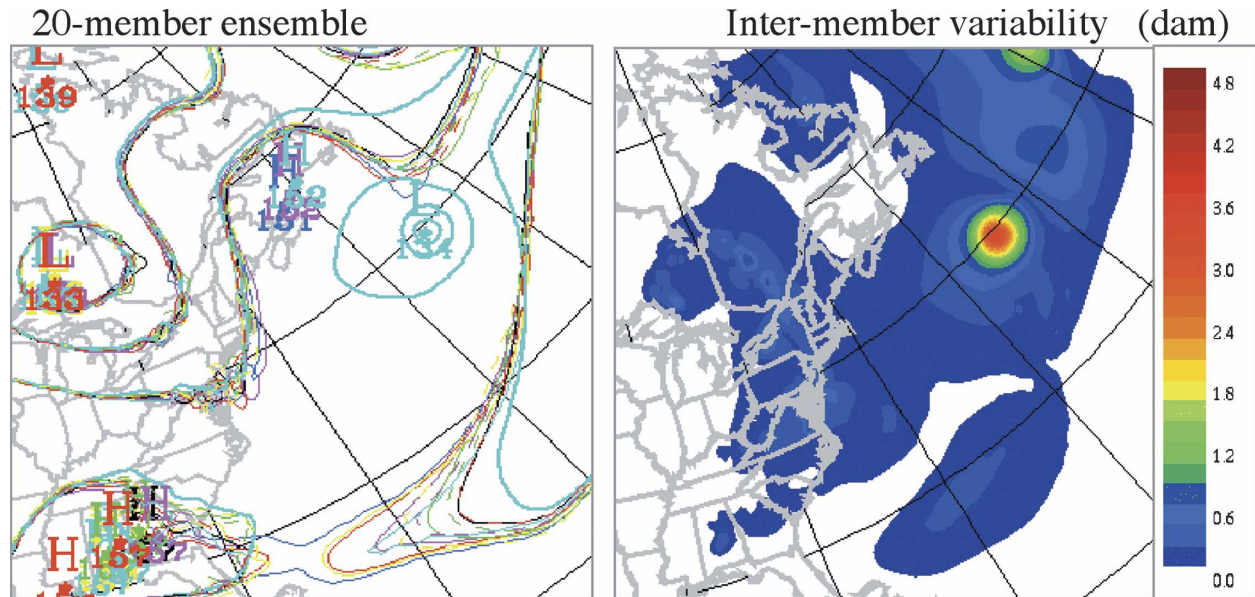


FIG. 16. Bimodal solutions (20-member ensemble, domain  $120 \times 120$ ): particular case of (left) one extreme deviation (blue) detected in the time evolution of the 850-hPa geopotential height (dam) and (right) the intermember variability  $\sqrt{\sigma_{\text{en}}^2}$  (dam) corresponding to this case (valid at 0000 UTC 25 Jul 1993).

#### 4. Conclusions

The purpose of this work was to describe and assess the importance of the internal variability in a nested RCM. To this aim, ensembles of 20 simulations were performed over five different domain sizes. Each of the 20 simulations was driven by the same set of time-dependent LBCs taken from NCEP–NCAR reanalyses using prescribed SSTs. The different members of the ensembles were initialized at 1-day intervals; the simulations were performed with the Canadian RCM (CRCM) for one summer season over the east coast of North America.

Internal variability is defined as the spread between the members during the integration period. The results show that internal variability depends strongly on synoptic events, as seen by the pulsating behavior of its time evolution. Internal variability displays a preferential region within the domain, depending on the variable. For example, precipitation, which is a difficult variable to simulate accurately (Kunkel et al. 2002), shows the largest variability in the southeast United States, where large convective precipitation occurs, while the 850-hPa geopotential height variability is largest in the northeast part of the domain corresponding to the downstream region. Evaluation of the time evolution of the synoptic patterns suggests that the maxima of variability in precipitation and 850-hPa geopotential height may be linked: the former, mostly located in the

southeast United States, acts as a triggering mechanism for the latter, which continues to develop along the storm track and reaches its maximum toward the northeast of the domain. This study confirms earlier results that internal variability increases with domain size. The study also shows that changes to the domain size may alter considerably the geographical distribution of the internal variability.

The repercussions of internal variability are also felt on seasonal-mean quantities. This suggests that one-season statistics of simulated fields, especially precipitation, may be poorly estimated from a single simulation. Our results indicate that a minimum number of 10 members are required for a robust estimation of a seasonal-mean value for midlatitude summer in certain areas where larger internal variability develops within the large domains. The study suggests that a reduction of the domain size generally results in a significant reduction of the differences between the members' statistics. There remain, however, regions with substantial internal variability magnitude, even at the seasonal scale.

A closer look at the evolution of the members in the ensembles reveals the occasional occurrence of bimodal solutions for the largest domains, during episodes of large internal variability. Model bimodal solutions could be the consequence of dynamical conditions that favor certain states (Lorenz 1963; Plu and Arbogast 2005), or could simply be the effect of poor sampling of the distribution with only 20 members. In any case, it is

850-hPa Geopotential height

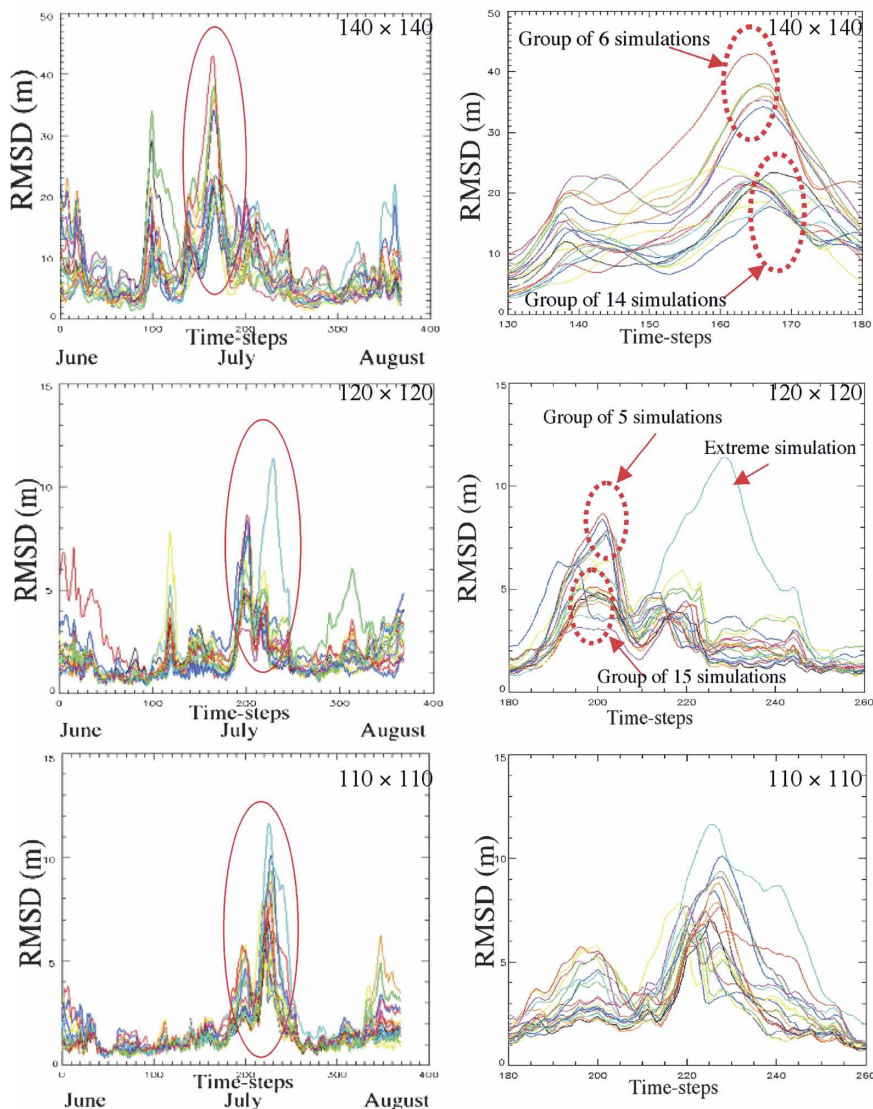


FIG. 17. Bimodal solution experiment: (left) RMSD time series for the 850-hPa geopotential height (m) and (right) a “zoom” of the main RMSD time series computed for domain sizes of 140 × 140, 120 × 120, 110 × 110, 100 × 100, and 80 × 80 grid points.

clear that undersampling may have important consequences on the estimation of the internal variability, as shown in the case of a strong low pressure system detected by only 1 member of the 20-member ensemble. The presence of bimodal solutions and of extreme cases far from the rest of the solutions suggests that patterns of internal variability may behave in a non-Gaussian way.

It is important to mention that large-scale nudging has been shown to be partially successful in diminishing the internal variability effects as well as the dependence on domain size (e.g., Weisse and Feser 2003; Miguez-

Macho et al. 2003). It is far from clear, however, how much of the internal variability within a model may be considered as “healthy,” and how much as “to be avoided.”

*Acknowledgments.* This research was done as a project within the Canadian Regional Climate Modelling Network (CRCM), which is financially supported by the Canadian Foundation for Climate and Atmospheric Sciences (CFCAS) and the Ouranos Consortium on Regional Climatology and Adaptation to Climate Change. We are also thankful to Dr. Daniel Caya

for useful discussions and collaboration, and to Claude Desrochers for maintaining a user-friendly computing environment. Similarly, we thank Hans von Storch and two anonymous reviewers for their helpful comments.

## REFERENCES

- Bechtold, P., E. Bazile, F. Guichard, P. Mascart, and E. Richard, 2001: A mass flux convection scheme for regional and global models. *Quart. J. Roy. Meteor. Soc.*, **127**, 869–886.
- Bergeron, G., L. Laprise, and D. Caya, 1994: Formulation of the Mesoscale Compressible Community (MC2) model. Cooperative Centre for Research in Mesometeorology Internal Rep., Montréal, QC, Canada, 165 pp.
- Castro, C. L., R. A. Pielke Sr., and G. Leoncini, 2005: Dynamical downscaling: Assessment of value retained and added using the Regional Atmospheric Modeling System (RAMS). *J. Geophys. Res.*, **110**, D05108, doi:10.1029/2004JD004721.
- Caya, D., and R. Laprise, 1999: A semi-implicit semi-Lagrangian regional climate model: The Canadian RCM. *Mon. Wea. Rev.*, **127**, 341–362.
- , and S. Biner, 2004: Internal variability of RCM simulations over an annual cycle. *Climate Dyn.*, **22**, 33–46.
- Christensen, O. B., M. A. Gaertner, J. A. Prego, and J. Polcher, 2001: Internal variability of regional climate models. *Climate Dyn.*, **17**, 875–887.
- Davies, H. C., 1976: A lateral boundary formulation for multilevel prediction models. *Quart. J. Roy. Meteor. Soc.*, **102**, 405–418.
- Fiorino, M., cited 2004: AMIP II sea surface temperature and sea ice concentration observations. [Available online at [http://www.pcmdi.llnl.gov/projects/amip/AMIP2EXPDSN/BCS\\_OBS/amip2\\_bcs.htm](http://www.pcmdi.llnl.gov/projects/amip/AMIP2EXPDSN/BCS_OBS/amip2_bcs.htm).]
- Gal-Chen, T., and R. C. J. Somerville, 1975: On the use of a coordinate transformation for the solution of the Navier–Stokes equations. *J. Comput. Phys.*, **17**, 209–228.
- Giorgi, F., 1990: Simulation of regional climate using a limited area model nested in a general circulation model. *J. Climate*, **3**, 941–963.
- , and L. O. Mearns, 1991: Approaches to regional climate change simulation: A review. *Rev. Geophys.*, **29**, 191–216.
- , and X. Bi, 2000: A study of internal variability of a regional climate model. *J. Geophys. Res.*, **105**, 29 503–29 521.
- Griffies, S. M., and K. Bryan, 1997: A predictability study of simulated North Atlantic multidecadal variability. *Climate Dyn.*, **13**, 459–487.
- Ji, Y., and A. D. Vernekar, 1997: Simulation of the Asian summer monsoons of 1987 and 1988 with a regional model nested in a global GCM. *J. Climate*, **10**, 1965–1979.
- Kain, J. S., and J. M. Fritsch, 1990: A one-dimensional entraining/detraining plume model and application in convective parameterization. *J. Atmos. Sci.*, **47**, 2784–2802.
- Kalnay, E., and Coauthors, 1996: The NCEP–NCAR 40-Year Reanalysis Project. *Bull. Amer. Meteor. Soc.*, **77**, 437–471.
- Kunkel, E., and Coauthors, 2002: Observations and regional climate model simulations of heavy precipitation events and seasonal anomalies: A comparison. *J. Hydrol.*, **3**, 322–334.
- Laprise, R., D. Caya, G. Bergeron, and M. Giguère, 1997: The formulation of André Robert MC2 (Mesoscale Compressible Community) model. *Atmos.–Ocean*, **35**, 195–220.
- Lorenz, E., 1963: Deterministic nonperiodic flow. *J. Atmos. Sci.*, **20**, 130–141.
- Lucas-Picher, P., D. Caya, and S. Biner, 2004: RCM's internal variability as function of domain size. *Research Activities in Atmospheric and Oceanic Modelling*, J. Côté, Ed., World Meteorological Organization, 7.27–7.28.
- McFarlane, N. A., G. J. Boer, J.-P. Blanchet, and M. Lazare, 1992: The Canadian Climate Centre Second-Generation General Circulation Model and its equilibrium climate. *J. Climate*, **5**, 1013–1044.
- Miguez-Macho, G., G. L. Stenchikov, and A. Robock, 2003: Spectral nudging to eliminate the effects of domain position and geometry in regional climate model simulations. *J. Geophys. Res.*, **109**, D13104, doi:10.1029/2003JD004495.
- Plu, M., and Ph. Arbogast, 2005: A cyclogenesis evolving into two distinct scenarios and its implications for short-term ensemble forecasting. *Mon. Wea. Rev.*, **133**, 2016–2029.
- Riette, S., and D. Caya, 2002: Sensitivity of short simulations to the various parameters in the new CRCM spectral nudging. *Research Activities in Atmospheric and Oceanic Modelling*, H. Ritchie, Ed., World Meteorological Organization, 39–40.
- Rinke, A., and K. Dethloff, 2000: On the sensitivity of a regional Arctic climate model to initial and boundary conditions. *Climate Res.*, **14**, 101–113.
- , P. Marbaix, and K. Dethloff, 2004: Internal variability in Arctic regional climate simulations: Case study for the SHEBA year. *Climate Res.*, **27**, 197–209.
- Seth, A., and F. Giorgi, 1998: The effects of domain choice on summer precipitation simulation and sensitivity in a regional climate model. *J. Climate*, **11**, 2698–2712.
- Vannitsem, S., and F. Chomé, 2005: One-way nested regional climate simulations and domain size. *J. Climate*, **18**, 229–233.
- von Storch, H., 2005: Models of global and regional climate. *Meteorology and Climatology*, M. G. Anderson, Ed., *Encyclopedia of Hydrological Sciences*, Vol. 1, Wiley, 478–490.
- , H. Langenberg, and F. Feser, 2000: A spectral nudging technique for dynamical downscaling purposes. *Mon. Wea. Rev.*, **128**, 3664–3673.
- Weisse, R., and F. Feser, 2003: Evaluation of a method to reduce uncertainty in wind hindcasts performed with regional atmosphere models. *Coastal Eng.*, **48**, 211–255.
- , H. Heyen, and H. von Storch, 2000: Sensitivity of a regional atmospheric model to a sea state-dependent roughness and the need of ensemble calculations. *Mon. Wea. Rev.*, **128**, 3631–3642.
- Wu, W., A. H. Lynch, and A. Rivers, 2005: Estimating the uncertainty in a regional climate model related to initial and boundary conditions. *J. Climate*, **18**, 917–933.